COMMUNICATIONS CHEMISTRY

ARTICLE

https://doi.org/10.1038/s42004-019-0242-0 OPEN

Polarizability and isotope effects on dispersion interactions in water

Yi-Yang Zhan [1], Qi-Chun Jiang[1], Kentaro Ishii [2], Takuya Koide[3], Osamu Kobayashi[3], Tatsuo Kojima [1], Satoshi Takahashi [1], Masanori Tachikawa [3], Susumu Uchiyama [2,4] & Shuichi Hiraoka [1*]

True understanding of dispersion interaction in solution remains elusive because of difficulty in the precise evaluation of its interaction energy. Here, the effect of substituents with different polarizability on dispersion interactions in water is discussed based on the thermodynamic parameters determined by isothermal titration calorimetry for the formation of discrete aggregates from gear-shaped amphiphiles (GSAs). The substituents with higher polarizability enthalpically more stabilize the nanocube, which is due to stronger dispersion interactions and to the hydrophobic effect. The differences in the thermodynamic parameters for the nanocubes from the GSAs with CH_3 and CD_3 groups are also discussed to lead to the conclusion that the H/D isotope effect on dispersion interactions is negligibly small, which is due to almost perfect entropy-enthalpy compensation between the two isotopomers.

[1] Department of Basic Science, Graduate School of Arts and Sciences, The University of Tokyo, 3-8-1 KomabaMeguro-kuTokyo 153-8902, Japan. [2] Exploratory Research Center on Life and Living Systems (ExCELLS), National Institutes of Natural Sciences, 5-1 Higashiyama, Myodaiji-cho, Okazaki, Aichi 444-8787, Japan. [3] Quantum Chemistry Division, Graduate School of Science, Yokohama City University, 22-2 Seto, Kanazawa-ku, Yokohama, Kanagawa 236-0027, Japan. [4] Department of Biotechnology, Graduate School of Engineering, Osaka University, 2-1 YamadaokaSuitaOsaka 565-0871, Japan. *email: chiraoka@mail.ecc.u-tokyo.c.jp

The dispersion force is a ubiquitous attractive interaction between atoms or molecules in close vicinity, as the potential energy of dispersion interaction (U) is expressed by $U \propto r^{-6}$, where r is the contact distance[1]. The dispersion force is branded as one of the weakest molecular interactions. However, as seen in gecko's foot for example[2,3], nature efficiently utilizes this molecular interaction. Such splendid examples have recently stimulated the utilization of dispersion interaction in artificial systems[4–12]. As the theoretical formalism of dispersion interactions indicates ($U(r) \propto \alpha_A \cdot \alpha_B / r^6$, where α_A, α_B, r are the polarizabilities of atoms A and B, and their distance, respectively), a large dispersion interaction works between two atoms with high polarizability[13]. However, the long atomic distances between such atoms with large atomic radius diminish the effect of polarizability[14]. Moreover, many-body interactions among molecules with more complex shape than spherical atoms make understating of dispersion interactions between molecules unclear. The dispersion interaction between two atoms or small molecules is too weak to evaluate its interaction energy[15]. The solvation of the molecules of interest, which contains more or less dispersion and other molecular interactions between solvent and solute, disturbs quantitative evaluation of the dispersion interactions between the solutes. Therefore, true understanding of dispersion interaction in solution remains elusive.

Here we report the polarizability effect on dispersion interactions in water based on the thermodynamic parameters determined by isothermal titration calorimetry (ITC) for discrete hydrophobic assemblies from structurally similar building blocks that possess substituents with different polarizability (CH_3, Cl, Br, and I). It was found that the association constant for the formation of the aggregates assembled from gear-shaped building blocks containing substituents with different polarizability was significantly altered (10^{18}–10^{25} M^{-5}) and that the assemblies with more polarizable substituents are enthalpically more stable, which is due to dispersion interactions with the contributions from the hydrophobic effect to some extent. On the other hand, enthalpically more stabilized assemblies are entropically destabilized. As the enthalpic contribution is larger than the entropic disadvantage, the introduction of polarizable substituents leads to thermodynamically more stable assemblies in water. The H/D isotope effect on dispersion interactions, whose understanding is still under discussion, was also investigated. The differences in ΔH and ΔS values for the nanocubes with protiums (H) and with deuteriums (D) are as small as the experimental errors, indicating that the H/D isotope effect on dispersion interaction is negligibly small.

Results

Molecular design of building blocks. Previously, we reported cube-shaped discrete molecular self-assemblies, i.e., nanocubes, from gear-shaped amphiphiles (GSAs) in water[16,17]. The main driving force of the self-assembly of the nanocubes is the hydrophobic effect, but weak intermolecular interactions such as dispersion[18] and cation-π[19] interactions also significantly contribute to the stability of the nanocubes. The accumulation of multiple weak interactions give rise to great thermal stability of the nanocubes, which do not disassemble into the monomers at all at even higher temperature than the boiling point of water[17]. These stable nanocubes are attractive for their use towards molecular functions[20,21,22], but their extremely high stability prevents us from determining the thermodynamic parameters for the self-assembly of the nanocubes to precisely discuss the effect of the weak intermolecular interactions. To slightly decrease the stability of the nanocube, we designed GSAs where a methoxy group is introduced on the periphery of the hexaphenylbenzene (HPB) core (Fig. 1a). When the methoxy group of **1-CH$_3$** is replaced with a benzene ring, the resulting nanocube from this GSA is very stable (decomposition temperature is 130 °C) due to triply stacked cation-π interactions, where the benzene ring is placed in between the two pyridinium rings (Py^+)[17].

The symmetry of the nanocube belongs to an S_6 point group (Fig. 1b); all the six GSAs in the nanocube are chemically equivalent. The symmetry of each GSA in the nanocube is C_1, indicating that all the three substituents X in the GSA are chemically inequivalent. If we compare the nanocube to the Earth, one of the substituents (X) in the GSA is placed around the poles, while the other two reside on the equator (red broken line in Fig. 1b). According to the energy-minimized structure of the (**1-CH$_3$**)$_6$ nanocube that was optimized from the crystal structure of the nanocube reported previously (the methoxy group in **1-CH$_3$** is replaced with 3-pyridyl group)[16], the three chemically inequivalent substituents (X) contact with the molecular surface of other GSAs in the nanocube (Fig. 1c), suggesting that the dispersion interactions around X play a significant role on the stability of the nanocube. As the twelve substituents (X) along the equator (X^E) are denser than the six substituents around the poles (X^P), the dispersion interactions (X···X and X···π) around X^E is likely to be stronger[23].

The dispersion interactions and the hydrophobic effect around X in the nanocube are simply expressed by the following equation.

$$X\cdots S + A\cdots S \rightleftarrows X\cdots A + S\cdots S \quad (1)$$

where A indicates X or aromatic rings in the GSA that interact with X. S indicates solvent molecules (H_2O). Thus, the free energy change in Eq. (1) is expressed by Eq. (2).

$$\Delta G(X) = G(X\cdots A) + G(S\cdots S) - G(X\cdots S) - G(A\cdots S) \quad (2)$$

The energy difference between the nanocubes with the substituents X^1 ($\Delta G(X^1)$) and X^2 ($\Delta G(X^2)$), which is indicated as $\Delta\Delta G$, is expressed by Eq. (3).

$$\Delta\Delta G = \Delta G(X^1) - \Delta G(X^2) = \Delta G_{disp} - \Delta G_{solv} \quad (3)$$

where ΔG_{disp} and ΔG_{solv} are defined as follows:

$$\Delta G_{disp} = G(X^1\cdots A) - G(X^2\cdots A) \quad (4)$$

$$\Delta G_{solv} = G(X^1\cdots S) - G(X^2\cdots S) \quad (5)$$

The contribution of the hydrophobic effect is proportional to the desolvation surface area[24–32], which is the difference in the solvent accessible surface areas (SAS) between the monomers and the aggregate (ΔSAS), and is estimated to be 100–200 J mol^{-1} Å^{-2}. Thus, when the substituents (X^1 and X^2) have a similar size, ΔSAS is negligibly small to lead to $\Delta G_{solv} \approx 0$. In this case, the change in the thermodynamic stability of the nanocubes assembled from a series of GSAs with different substituents (X) allows us to discuss dispersion interactions based on the thermodynamic parameters for the formation of the nanocubes. However, the size of substituents (X = CH_3, Cl, Br, and I) is inevitably different, so the experimentally obtained $\Delta\Delta G$ values should contain the contribution of the hydrophobic effect to some extent. Although the difference in the ΔSAS values between the nanocubes assembled from GSAs ((**1-X**)$_6$ (X = CH_3, CD_3, Cl, Br, and I)) is less than 125 Å^2, which is about 7% of the ΔSAS for the nanocubes (Table 1), the experimentally obtained free energy changes of the nanocubes are largely different, ranging from −103 to −143 kJ mol^{-1}. Under the assumption that the difference in the ΔG values is caused by only the hydrophobic effect, the contribution of the hydrophobic effect per Å^2 is calculated to be 320 J mol^{-1} Å^{-2},

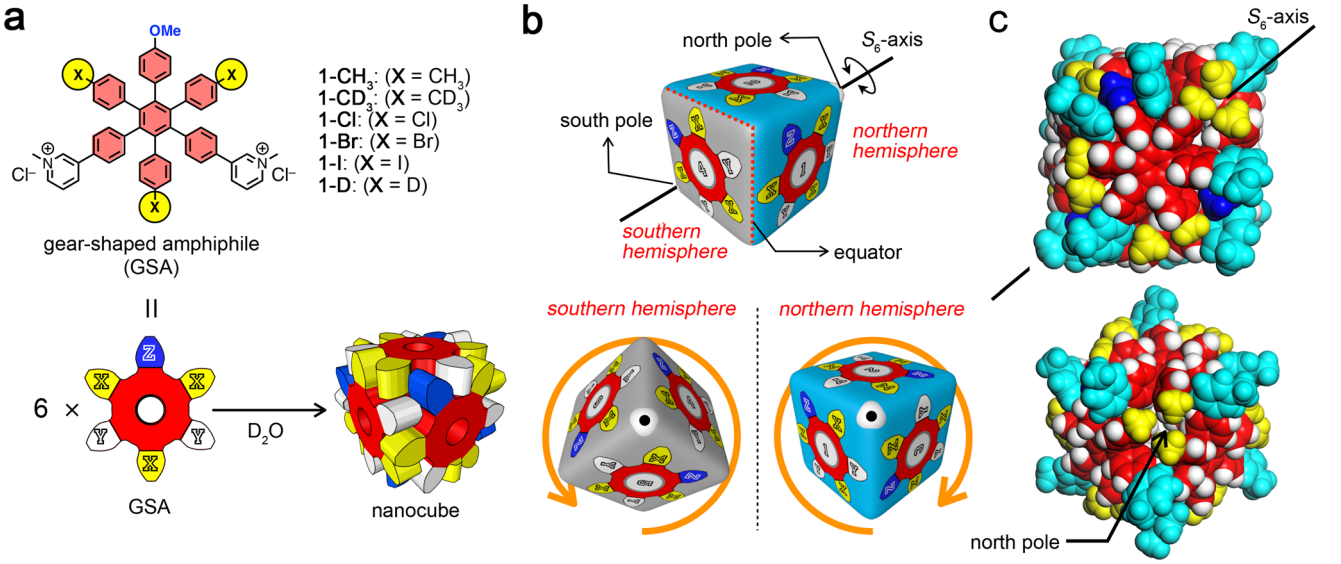

Fig. 1 Structural features of the nanocubes. a Chemical structures of gear-shaped amphiphiles (GSAs) **1-X** (X = CH_3, CD_3, Cl, Br, I, and D) and their assembly into hexameric molecular boxes, nanocube. **b** The structure of the nanocube compared to the Earth. The S_6-axis of the nanocube corresponds to the axis of the Earth. The two apexes penetrated by the S_6-axis corresponds to the north and south poles. The six sides that do not contain the poles (red broken line) indicates the equator of the nanocube. The three GSAs in the northern hemisphere are arranged in a clockwise direction, while those in the southern hemisphere are in a counterclockwise direction. Three substituents (X) around the north or south pole are close to each other. The other twelve substituents (X) along the equator are six pairs where the two substituents are close to each other. **c** Energy-minimized structure of the $(\mathbf{1\text{-}CH_3})_6$ nanocube. Red and white indicate carbon and hydrogen atoms of the hexaphenylbenzene core, respectively. Yellow, blue, and cyan indicate substituents (X = CH_3), methoxy groups, and *N*-methyl pyridinium rings, respectively.

which is 1.6–3.2 times larger than the hydrophobic contribution reported in the previous research.[24–32] Therefore, the contribution from the hydrophobic effect cannot perfectly be excluded in this system, but the difference between the ΔG values for the nanocubes is certainly affected by the difference in the polarizability of the substituent X.

The advantage of the use of the nanocubes to discuss weak intermolecular interactions is that even though the stabilization energy arising from one substituent X is as small as is difficult to evaluate, such a very small contribution can be accumulated by 18 atoms or groups of X in the nanocubes to lead to detectable energy differences. Furthermore, the dispersion interactions can be discussed based on the thermodynamic parameters determined by dilution ITC measurement for the self-assembly of the nanocubes.

Self-assembly of nanocubes from gear-shaped amphiphiles. Six C_{2v}-symmetric GSAs (**1-X** (X = CH_3, CD_3, Cl, Br, I, and D)) designed in this research (Fig. 1a) were synthesized based on two strategies using (1) alternately trilithiated HPB derivatives[33,34] for **1-CH$_3$**, **1-CD$_3$**, **1-Br**, **1-I**, and **1-D** and (2) pentasubstituted pyrylium salts[35] for **1-Cl** (Supplementary Methods). Although the ^{1}H NMR spectra of the GSAs (**1-CH$_3$**, **1-Cl**, **1-Br**, and **1-I**) measured in CD_3OD showed simple patterns, indicating the monomers, those measured in D_2O were more complicated than expected from C_{2v}-symmetric GSA structures. The aliphatic (methoxy, *N*-methyl, and *p*-tolyl (for **1-CH$_3$**)) and some of the aromatic proton signals appeared further upfield compared to those of the monomers, suggesting the formation of molecular aggregates by the hydrophobic effect. The ^{1}H NMR spectrum of **1-CH$_3$** in D_2O showed chemically inequivalent three *p*-tolyl methyl signals in a 1:1:1 ratio and two *N*-methyl signals in a 1:1 ratio (Fig. 2). Similarly, only one set of two kinds of *N*-methyl signals in a 1:1 ratio was observed in the ^{1}H NMR spectra of other GSAs (**1-Cl**, **1-Br**, and **1-I**) in D_2O. These ^{1}H NMR spectral patterns are consistent with the C_1-symmetric GSA in the crystal structure of the nanocube reported previously[16] (Fig. 1c and Supplementary Fig. 27). ^{1}H DOSY spectroscopy of the nanocubes from **1-CH$_3$**, **1-Cl**, **1-Br**, and **1-I** revealed the diffusion coefficient (D) of about 1.23×10^{-10} m^2 s^{-1} (Supplementary Figs. 4, 8, 12, and 14), which is similar to that of the previously reported nanocube ($D = 1.28 \times 10^{-10}$ m^2 s^{-1})[17]. ESI-TOF mass spectrometry of aqueous solutions of the GSAs except **1-Cl** in the presence of H_2SO_4[17] detected the signals of the hexamers as negatively charged species (Supplementary Fig. 21 and Supplementary Table 1). These results indicate that GSAs (**1-CH$_3$**, **1-Cl**, **1-Br**, and **1-I**) assembled into hexameric aggregates (the nanocubes) in water.

The ^{1}H NMR spectrum of **1-D** in D_2O showed broadening of the signals, some of which were slightly shifted upfield. These results suggest that **1-D** also assembled into a certain aggregate by the hydrophobic effect. The D value of the aggregate from **1-D** in D_2O (1.63×10^{-10} m^2 s^{-1}) is larger than that of the nanocubes (Supplementary Fig. 17). ESI-TOF mass measurement of an aqueous solution of **1-D** with H_2SO_4 showed the signals of the hexamer. Although a clear ^{1}H NMR spectrum was not obtained even at a low temperature (283 K) (Supplementary Fig. 16), the addition of 1,3,5-tribromomesitylene in an aqueous solution of **1-D** led to a clear ^{1}H NMR spectrum of the nanocube that encapsulates two guest molecules in its hydrophobic cavity[16,17] (Supplementary Fig. S15). These results indicate that the aggregate assembled from **1-D** in D_2O, which would be the $(\mathbf{1\text{-}D})_6$ nanocube, is structurally more dynamic and less stable. The solvent accessible surface (SAS) area of **1-D**, 1125.6 Å^2, is comparable with those of the other GSAs (1186.8–1234.5 Å^2) and the shape of GSA **1-D** is very similar to those of the other GSAs (Table 1). Thus, if only the hydrophobic effect determines the stability of the nanocubes, the $(\mathbf{1\text{-}D})_6$ nanocube should be more stable than observed. Therefore, the stabilization of the nanocubes is affected not only by the hydrophobic effect (mainly determined by the number of desolvated water molecules) but also by other attractive

Table 1 Thermodynamic parameters and related values for the formation of the nanocubes.

GSA	α[a] [Å^3]	SAS[b] [Å^2]	ΔSAS[c] [Å^2]	K_a[d] [M^{-5}]	ΔG[d] [kJ mol^{-1}]	ΔH[d] [kJ mol^{-1}]	-298·ΔS[d] [kJ mol^{-1}]
1-CH$_3$	2.60[e]	1207.2	1879.3	6.31×10^{22}	−130.1 ± 0.0	−78.1 ± 0.6	−52.0 ± 0.6
1-CD$_3$	—	n.d.[f]	n.d.[f]	7.94×10^{22}	−130.6 ± 0.0	−74.8 ± 0.5	−55.8 ± 0.5
1-Cl	2.18	1186.8	1854.6	1.00×10^{18}	−102.7 ± 0.0	−69.2 ± 1.0	−33.5 ± 1.0
1-Br	3.05	1206.5	1909.5	1.26×10^{21}	−120.4 ± 0.0	−97.0 ± 1.3	−23.3 ± 1.3
1-I	4.70	1234.5	1978.4	1.26×10^{25}	−143.2 ± 0.6	−125.6 ± 1.1	−17.6 ± 1.7
1-D	—	1125.6	1570.1	n.d.[f]	n.d.[f]	n.d.[f]	n.d.[f]

[a]Polarizability of substituent X[35]
[b]Solvation surface area of monomer GSA determined by using probe sphere of 2.8 Å in diameter
[c]ΔSAS indicates the half of the difference of the solvation surface area between six monomer GSAs and the nanocube determined by using probe sphere of 2.8 Å in diameter
[d]Determined by dilution ITC measurements at 298 K. The experiments were carried out three times
[e]Polarizability of CH_4
[f]Not determined

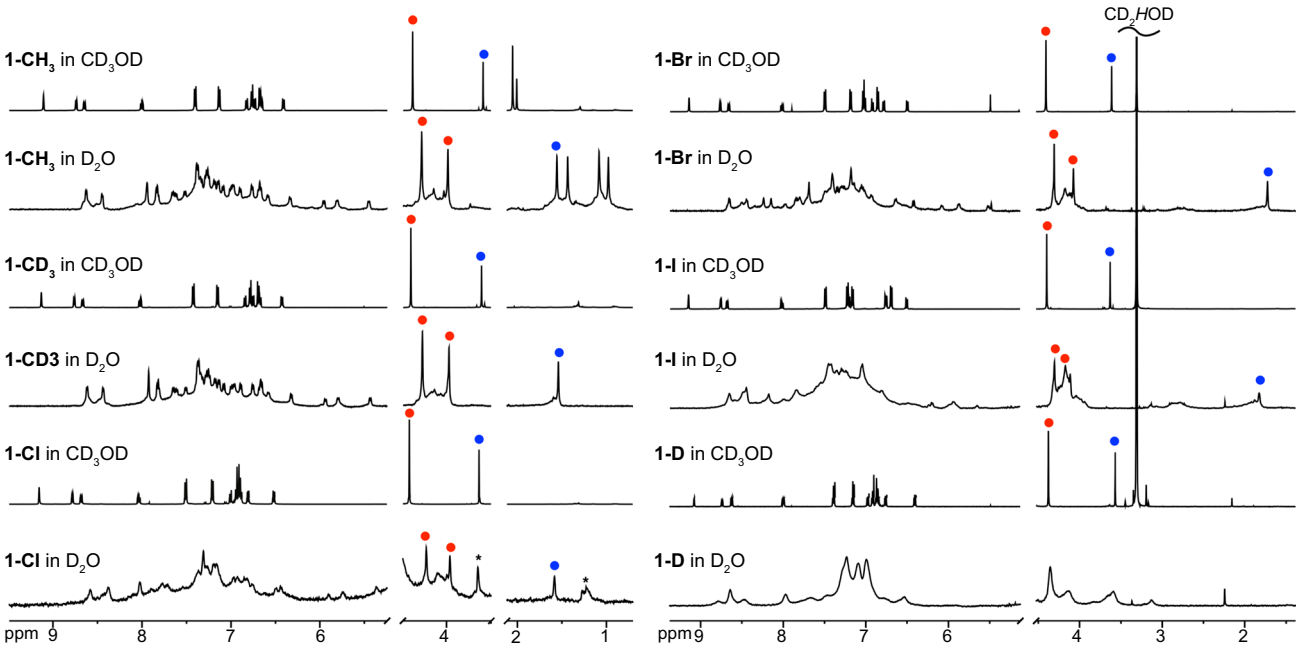

Fig. 2 ^{1}H NMR spectra of gear-shaped amphiphiles and their aggregates, nanocubes. ^{1}H NMR (500 MHz, 298 K) spectra of the monomer state of the gear-shaped amphiphiles (GSAs) **1-X** (X = CH_3, CD_3, Cl, Br, I, and D) were measured in CD_3OD ([GSA] = 1.0 mM), while those of nanocubes were in D_2O ([GSA] = 1.0 mM). Blue and red solid circles indicate methoxy and *N*-methyl signals, respectively. The assignment of the ^{1}H NMR signals is indicated in Supplementary Figs. 1–20.

interactions (dispersion interactions) working around the substituents X in the nanocubes. It is worth mentioning that the result that **1-D** assembled into the nanocube without help of the dispersion interactions around the substituents (X) suggests that the entropic penalty of the assembly of the GSAs has already been paid by the aggregation of the core part of the GSAs, which mainly causes the hydrophobic effect. Thus, the introduction of more polarizable substituents (X) in the GSAs stabilizes the nanocubes by stronger dispersion interactions and the hydrophobic effect.

Polarizability effect on the thermodynamic stability of the nanocubes. Thermodynamic parameters for the self-assembly of the nanocubes from GSAs (**1-CH$_3$**, **1-Cl**, **1-Br**, and **1-I**) were determined by dilution ITC measurements[17] (Table 1, Supplementary Figs. 22, 24–26 and Supplementary Tables 2, 4–6). In all cases, the experimental data could be analyzed as the transition between the monomers and the hexamer, which is consistent with the observation of only the two states by variable-temperature ^{1}H NMR spectroscopy[17]. The thermodynamic parameters for **1-D** could not be determined because of the low stability of its aggregate. For the hydrophobic assembly, ΔG value linearly correlate with ΔSAS[24–32]. In the case of the nanocubes with different substituents, although ΔSASs for the nanocubes are similar, their free energy changes for the self-assembly are largely different (Fig. 3a), suggesting that the change in the thermodynamic stability of the nanocube with different substituents (X) arises mainly from dispersion interactions around the substituents. The −ΔG value for **1-CH$_3$** is plotted higher than the linear relation for the nanocubes with halogen atoms (**1–Cl**, **1-Br**, and **1-I**) (Fig. 3a), which is partly due to the difference in the polarity of halogen atoms and methyl group. As more polar halogens are hydrated better than methyl groups, the assemblies are more stabilized by the desolvation of water molecules around less polar substituents.

When the dispersion interactions around substituents (X) contribute to the stability of the nanocubes, the enthalpy change (ΔH) should correlate with the polarizability of the substituents (X)[36], which is true as shown in Fig. 3b. If we assume that the contributions of the three chemically inequivalent substituents (X) of the GSA to the dispersion interactions in the nanocube are

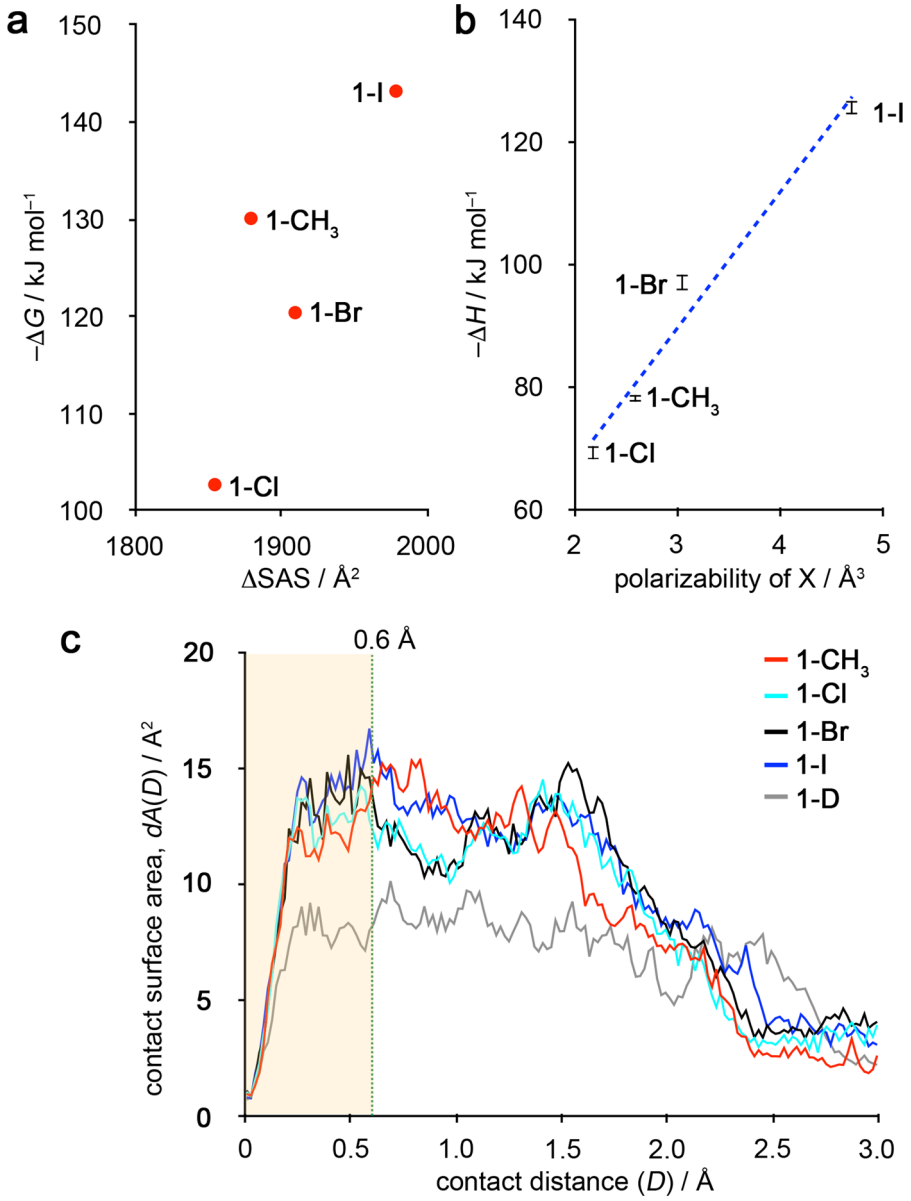

Fig. 3 Thermodynamic stability of the nanocubes. a A plot of log K_a values for the formation of the nanocubes ((**1-CH$_3$**)$_6$, (**1-Cl**)$_6$, (**1-Br**)$_6$, and (**1-I**)$_6$) against the desolvation surface area (ΔSAS). Although ΔSAS for (**1-CH$_3$**)$_6$, (**1-Cl**)$_6$, (**1-Br**)$_6$, and (**1-I**)$_6$ are similar, their stabilities are significantly different, indicating that the difference in the thermodynamic stabilities of the nanocubes is not due to the hydrophobic effect but to the dispersion interactions around the substituents (X). **b** A plot of the enthalpy change of the self-assembly of the nanocubes ((**1-CH$_3$**)$_6$, (**1-Cl**)$_6$, (**1-Br**)$_6$, and (**1-I**)$_6$) against the polarizability of X. For (**1-CH$_3$**)$_6$, the polarizability of CH_4 was used. Error bars indicate the standard deviation. **c** The distribution of the contact surface area (d$A(D)$) against the contact distance (D) (SAVPR) for the nanocubes (**1-CH$_3$**)$_6$, (**1-Cl**)$_6$, (**1-Br**)$_6$, and (**1-I**)$_6$.

the same, the dispersion interaction arising from one substituent changes linearly with the difference in the polarizability of X ($1.24 \times \Delta\alpha$ kJ mol^{-1}).

It was also found that the ΔH values linearly correlate with ΔSAS. This is mainly because the polarizability of the substituents (X) linearly correlates with ΔSAS. This relation is reasonable because more polarizable atom has larger atomic radius, so the ΔSAS value of the nanocube with more polarizable substituents is larger. Therefore, the change in the ΔH values by the substituents may partly contain the contribution of ΔSAS (the hydrophobic effect).

The entropy change for the self-assembly is positive for all the nanocubes, which is mainly due to the hydrophobic effect. The entropic substituent effect on the contribution to the stability of the nanocubes opposes the enthalpic one (Table 1), which is qualitatively explained by entropy-enthalpy compensation[37,38]; stronger binding gains a larger negative enthalpy change, while such tight binding restricts the translational and rotational freedom to lead to entropic disadvantage. In other words, the GSAs in the nanocube assembled from the GSAs with highly polarizable substituents (X) more tightly engage with each other by stronger dispersion interactions around X. The entropy change in the self-assembly of the nanocube in water is mainly composed of two factors: (1) the positive entropy change caused by desolvation of the energetically destabilized water molecules on the GSA surface (the hydrophobic effect) and (2) the negative entropy change caused by the restricted translational and rotational motions of the GSAs upon the self-assembly of the nanocube. As ΔSAS areas for the nanocubes are similar, the hydrophobic effect on the entropy change should also be similar.

Thus, the difference in the entropy change between the nanocubes is mainly due to the loss of the freedom of the GSAs in the nanocube. However, as discussed on the enthalpy change, the difference in ΔS value between the nanocubes would contain the hydrophobic contribution.

In order to analyze the molecular meshing between the GSAs in the nanocubes, SAVPR (surface analysis with varying probe radii)[18] was carried out. SAVPR shows the distribution of the contact surface area as a function of contact distance. As the size of a water molecule is as large as a sphere whose diameter is 2.8 Å, SAVPR for the contact distance shorter than 2.8 Å enables us to discuss the effect of molecular meshing (dispersion interactions), excluding the hydrophobic contribution. In molecular self-assemblies that have large contact surface area with short contact distances, the building blocks tightly mesh with each other, which are enthalpically favorable but entropically unfavorable. It was found in our previous analysis that the contact surface with contact distance shorter than at least 0.9 Å is important for molecular meshing.[18] Smaller contact surfaces area with short contact distance suggests weaker dispersion interactions, which lead to smaller enthalpy change, and higher motional freedom of the GSAs in the nanocube, which leads to larger entropy change. SAVPR data for the energy-minimized structures of the nanocubes are shown in Fig. 3c. It is obvious that the molecular meshing in the $(\mathbf{1\text{-}D})_6$ nanocube is quite low, which is consistent with its low thermodynamic stability. When we focus on the contact surface area with contact distance shorter than 0.6 Å for the nanocube ($(\mathbf{1\text{-}CH_3})_6$, $(\mathbf{1\text{-}Cl})_6$, $(\mathbf{1\text{-}Br})_6$, and $(\mathbf{1\text{-}I})_6$), the contact surfaces area with short contact distance increases in the order of $(\mathbf{1\text{-}CH_3})_6$ (304 Å^2) < $(\mathbf{1\text{-}Cl})_6$ (318 Å^2) < $(\mathbf{1\text{-}Br})_6$ (330 Å^2) < $(\mathbf{1\text{-}I})_6$ (345 Å^2), indicating that GSAs in the nanocube with a smaller entropy change more tightly mesh each other. Consequently, the nanocubes assembled from GSAs with more polarizable substituents (X) are enthalpically more stabilized, while the entropic contribution is smaller in such nanocubes. However, as the enthalpic contribution is larger than the entropic one, stronger dispersion interactions overcome the entropic penalty.

Isotope effect on dispersion interaction. Although a lot of efforts have been made[39–52], the H/D isotope effect on intermolecular interactions is still in debate. Under Born-Oppenheimer approximation, the potential energy surfaces of complexes with different isotope(s) are the same, so the difference in the thermodynamic stability between the two isotopomers arises from the vibrational frequency of C–H and C–D bonds. Due to smaller vibrational frequency of C–D bond, the average C–D bond distance is slightly shorter than the C–H bond distance by 0.005 Å and C–H bond is more polarizable than C–D bond[49–51]. The studies on the encapsulation of protic and deuterated guest molecules in molecular capsules led to the conclusion that CD···π interaction is stronger than CH···π interaction[39,40,52], while those based on chromatographic analysis led to the opposite conclusion[41,42]. Other studies indicate very small or nondetectable difference between the isotopes[43,53–55].

The H/D isotope effect on dispersion interactions was investigated by comparing the thermodynamic parameters of the $(\mathbf{1\text{-}CH_3})_6$ and $(\mathbf{1\text{-}CD_3})_6$ nanocubes (Table 1 and Supplementary Figs. 22 and 23 and Supplementary Tables 2 and 3). ΔG values for the two isotopomers are almost the same, which is consistent with the recent reports[43,53–55] on the H/D isotope effect. The differences in the ΔH and ΔS values between the $(\mathbf{1\text{-}CH_3})_6$ and $(\mathbf{1\text{-}CD_3})_6$ nanocubes are small, but the enthalpy change for $(\mathbf{1\text{-}CH_3})_6$ is slightly more negative than that for $(\mathbf{1\text{-}CD_3})_6$, even if the error is 2%, which is suggested for ITC measurements[56]. The smaller ΔH value for $(\mathbf{1\text{-}CH_3})_6$ is consistent with the fact that protium is more polarizable than deuterium. Under the assumption that all the substituents (X) equally contribute to the stability of the nanocube, the difference in the enthalpic contribution from one methyl group ($\Delta\Delta H$) is 0.18 kJ mol^{-1}. On the other hand, the entropic contribution for $(\mathbf{1\text{-}CH_3})_6$ is smaller than that for $(\mathbf{1\text{-}CD_3})_6$, even when 2% of error is assumed. The enthalpic advantage compensates for the entropic unfavorability in $(\mathbf{1\text{-}CH_3})_6$, resulting in very similar free energy changes for the two isotopomers. As a consequence, the dispersion enthalpy for protium is stronger than that for deuterium as is expected from the difference in the polarizability between the two isotopes, but almost perfect entropy–enthalpy compensation leads to a negligibly small difference in the stabilization free energy.

Discussion

In conclusion, the effect of polarizability on the dispersion interactions in water was investigated by comparing the thermodynamic parameters determined by dilution ITC measurements for the formation of discrete aggregates (nanocubes) assembled from GSAs possessing three substituents (X) with different polarizability (X = Cl, Br, I, CH_3, and CD_3). As the desolvation surface areas for the nanocubes are not largely different, the difference in the thermodynamic parameters is affected by the difference in the dispersion interactions of the substituents (X) with different polarizability, though the contribution from the hydrophobic effect contains to some extent. This indicates that the polarizability effect is larger than the atom size effect on the dispersion interaction ($U(r) \propto \alpha_A \cdot \alpha_B / r^6$). The stabilization energy of weak molecular interactions is difficult to precisely determine by experiment. In the molecular self-assembly system presented here, detectable energy differences were obtained by the accumulation of 18 substituents (X) in the nanocube, whose assembly and disassembly are simply expressed as the transition between the two states (monomers and hexamer). The nanocubes were stabilized by the introduction of more polarizable substituents, showing a linear relation between the enthalpy change and the polarizability of X. The enthalpic contribution from more polarizable substituents is greater than the entropic penalty, which results in stronger dispersion interactions with the molecular surface of other GSAs in the nanocube. The H/D isotope effect on dispersion interactions is also interpreted by the polarizability of the two isotopes. In terms of enthalpy, protium makes dispersion interactions slightly stronger than deuterium, but the dispersion free energies caused by the two isotopes are almost the same due to entropy–enthalpy compensation, which is the different behavior between the effect of H/D isotopes and of halogen atoms.

Methods

General. ^{1}H, ^{13}C, and 2D NMR spectra were recorded using a Bruker AV-500 (500 MHz) spectrometer. Chemical data are reported in parts per million (ppm, δ scale) downfield from tetramethylsilane (δ 0.00) and are referenced to proton resonance of a residual peak of NMR solvents. The data are presented as follows: chemical shifts, multiplicity (s = singlet, d = doublet, t = triplet, q = quartet and/or multiplet resonances), coupling constants in Hertz (Hz), and integration. High-resolution mass spectra (HRMS) were obtained using a Waters Xevo G2-S QTOF mass spectrometer. Mass spectra of the nanocubes were recorded on a SYNAPT G2-S*i* HDMS mass spectrometer (Waters, Massachusetts, Milford, USA). Column chromatography was carried out with Merck Silica gel 60 (0.063–0.200 mm) unless otherwise noted. Gel permeation liquid chromatography (GPC) was performed using a Japan Analytical Industry LC-9204 with JAIGEL 2HR + 2.5HR columns using chloroform as a solvent. Dilution isothermal titration calorimetry (ITC) experiments were conducted on a Malvern MicroCal iTC200.

Materials. Unless otherwise noted, all solvents and reagents were obtained from commercial suppliers (TCI Co., Ltd., WAKO Pure Chemical Industries Ltd., KANTO Chemical Co., Inc., and Sigma-Aldrich Co.) and were used as received.

Compound 2[33] and 10[57] were prepared according to the literatures. NMR spectra are available in Supplementary Figs. 28–75.

ESI-TOF mass measurement of the nanocubes. For the confirmation of the assembly of the nanocubes, electrospray ionization-time-of-flight (ESI-TOF) mass spectrometry was performed according to our previous reports[17] with minor modifications. The concentrations of GSAs containing 1 mM H_2SO_4 were 0.9 mM. Capillary voltage and backing pressure are 0.93 kV and 0.13 bar. The other conditions are the same as are previously reported. Briefly, mass spectra were recorded on a SYNAPT G2-S*i* HDMS mass spectrometer (Waters, Massachusetts, Milford, USA) in negative ionization mode with a 0 V sampling cone voltage and source offset voltage, 4 V trap and 2 V transfer collision energy, and 1.5 mL/min trap gas flow. The samples added 1 mM H_2SO_4 were immediately injected into gold-coated glass capillaries made in house (approximately 5 μL sample loaded per analysis) and measured. The spectra were calibrated using 1 mg/mL cesium iodide and analyzed using MassLynx software (Waters).

Dilution ITC experiments. Dilution isothermal titration calorimetry (ITC) experiments were conducted on a Malvern MicroCal iTC_{200}. The calorimetric cell was filled with H_2O (0.2047 mL). Before every ITC experiment, the concentration of the nanocube in H_2O solution was determined to be about 2 mM by ^1H NMR measurement with NMe_4Cl as an internal standard. For one titration experiment, totally 29 injections were performed and in each injection 1 μL of aqueous solution of the nanocube was added except the first injection, 0.2 μL, which was discarded in all the experiments. An interval time of 150 s between each injection was applied to enable equilibration. The dataset was analysed by the modified Wittung-Stafshede's method to determine the dissociation constant K_D, the dissociation enthalpy, ΔH_D, and the heat of dilution, C[58]. The titration experiments were performed in triplicate to obtain the average value with the standard deviation.

Energy-minimized structure of nanocubes by molecular mechanics calculations. Geometry optimization for nanocubes in water and chloride ions was performed by molecular mechanics (MM) calculation with AMBER16 program package[59]. The X-ray structure of the nanocube (the methoxy group in **1-CH$_3$** is replaced with 3-pyridyl group)[16] was used as initial coordinate. The substituents on the X-ray structure of the **PM** nanocube were replaced to appropriate groups to construct the corresponding initial structures. For the nanocubes, we employed the general AMBER force field[60] and restrained electrostatic potential charges[61], based on the electrostatic potentials calculated with the HF/6-31G(d) method[62]. For water molecules and chloride ions, TIP4P/Ew force field[63] was used. The total numbers of water molecules were 9987, 9994, 9992, 9990, and 9994 for (**1-CH$_3$**)$_6$Cl$_{12}$, (**1-Cl**)$_6$Cl$_{12}$, (**1-Br**)$_6$Cl$_{12}$, (**1-I**)$_6$Cl$_{12}$ and (**1-D**)$_6$Cl$_{12}$ systems, respectively, and the number of chloride ions was 12. 20 water molecules and 1 chloride ion were encapsulated in the nanocubes. A virtual probe with a radius of 1.4 Å (water-sized) was employed to determine the SAS (solvent accessible surface) of nanocubes and six monomers.

Surface analysis with varying probe radii for the nanocubes. Surface analysis with varying probe radii (SAVPR)[18] was carried out as follows. Surface areas of the assembled and disassembled state, $A_{as}(D)$ and $A_{dis}(D)$, were calculated as the Connolly surface areas of the assembled and disassembled states with a probe sphere with a diameter of D, respectively, using Materials Studio software (version 8.0; Biovia Inc., USA). In this study, $dD = 0.02$ Å was adopted.

Data availability

The authors declare that all the other data supporting the findings of this study are available within the article and its supplementary information files and from the corresponding author upon request.

Received: 8 May 2019; Accepted: 20 November 2019;
Published online: 12 December 2019

References

1. Schneider, H.-J. Dispersive interactions in solution complexes. *Acc. Chem. Res.* **48,** 1815–1822 (2015).
2. Autumn, K. et al. Evidence for van der Waals adhesion in gecko setae. *Proc. Natl. Acad. Sci. USA* **99,** 12252–12256 (2002).
3. Ge, L., Sethi, S., Ci, L., Ajayan, P. M. & Dhinojwala, A. Carbon nanotube-based synthetic gecko tapes. *Proc. Natl Acad. Sci. USA* **104**, 10792–10795 (2007).
4. Grimme, S. & Schreiner, P. R. Steric crowding can stabilize a labile molecule: solving the hexaphenylethane riddle. *Angew. Chem. Int. Ed.* **50**, 12639–12642 (2011).
5. Ndambuki, S. & Ziegler, T. Analysis of the putative Cr–Cr quintuple bond in Ar′CrCrAr′ (Ar′ = C6H3-2,6(C6H3-2,6-Pri2)2 based on the combined natural orbitals for chemical valence and extended transition state method. *Inorg. Chem.* **51**, 7794–7800 (2012).
6. Guo, J.-D., Liptrot, D. J., Nagase, S. & Power, P. P. The multiple bonding in heavier group 14 element alkene analogues is stabilized mainly by dispersion force effects. *Chem. Sci.* **6**, 6235–6244 (2015).
7. Schreiner, P. R. et al. Overcoming lability of extremely long alkane carbon–carbon bonds through dispersion forces. *Nature* **477**, 308–311 (2011).
8. Yang, L., Brazier, J. B., Hubbard, T. A., Rogers, D. M. & Cockroft, S. L. Can dispersion forces govern aromatic stacking in an organic solvent? *Angew. Chem. Int. Ed.* **55**, 912–916 (2016).
9. Hwang, J., Li, P., Smith, M. D. & Shimizu, K. D. Distance–dependent attractive and repulsive interactions of bulky alkyl groups. *Angew. Chem. Int. Ed.* **55**, 8086–8089 (2016).
10. Adam, C., Yang, L. & Cockroft, S. L. Partitioning solvophobic and dispersion forces in alkyl and perfluoroalkyl cohesion. *Angew. Chem. Int. Ed.* **54**, 1164–1167 (2015).
11. He, S. et al. Cavitation energies can outperform dispersion interactions. *Nat. Chem.* **10**, 1252–1257 (2018).
12. Pollice, R., Bot, M., Kobylianskii, I. J., Shenderovich, I. & Chen, P. Attenuation of London dispersion in dichloromethane solutions. *J. Am. Chem. Soc.* **139**, 13126–13140 (2017).
13. Slater, J. C. & Kirkwood, J. G. The van der Waals forces in gases. *Phys. Rev.* **37**, 682–697 (1931).
14. Hunter, C. A. Quantifying intermolecular interactions: guidelines for the molecular recognition toolbox. *Angew. Chem. Int. Ed.* **43**, 5310–5324 (2004).
15. Yang, L., Adam, C., Nichol, G. S. & Cockroft, S. L. How much do van der Waals dispersion forces contribute to molecular recognition in solution? *Nat. Chem.* **5**, 1006–1010 (2013).
16. Hiraoka, S., Nakamura, T., Shiro, M. & Shionoya, M. In-water truly monodisperse aggregation of gear-shaped amphiphiles based on hydrophobic surface engineering. *J. Am. Chem. Soc.* **132**, 13223–13225 (2010).
17. Zhan, Y.-Y. et al. Hyperthermostable cube-shaped assembly in water. *Commun. Chem.* **1**, 14 (2018).
18. Tanaka, N. et al. Semi-quantitative evaluation of molecular meshing by surface analysis with varying probe radii. *Chem. Commun.* **54**, 3335–3338 (2018).
19. Zhan, Y.-Y., Kojima, T., Koide, T., Tachikawa, M. & Hiraoka, S. A balance between van der Waals and cation-π interactions that stabilizes hydrophobic assemblies. *Chem. Eur. J.* **24**, 9130–9135 (2018).
20. Zhan, Y.-Y. et al. Induced-fit expansion and contraction of a self-assembled nanocube finely responding to neutral and anionic guests. *Nat. Commun.* **9**, 4530 (2018).
21. Zhan, Y.-Y. et al. Temperature-controlled repeatable scrambling and induced-sorting of building blocks between cubic assemblies. *Nat. Commun.* **10**, 1440 (2019).
22. Zhan, Y.-Y. et al. Supramolecular fluorescence sensor for liquefied petroleum gas. *Commun. Chem.* **2**, 107 (2019).
23. Zhan, Y.-Y. et al. Importance of molecular meshing for the stabilization of solvophobic assemblies. *J. Org. Chem.* **83**, 5132–5137 (2018).
24. Hermann, R. B. Theory of hydrophobic bonding. II. Correlation of hydrocarbon solubility in water with solvent cavity surface area. *J. Phys. Chem.* **76**, 2754–2759 (1972).
25. Harris, S. M. J., Higuchi, T. & Rytting, J. H. Thermodynamic group contributions from ion pair extraction equilibriums for use in the prediction of partition coefficients. Correlation of surface area with group contributions. *J. Phys. Chem.* **77**, 2694–2703 (1973).
26. Reynolds, J. A., Gilbert, D. B. & Tanford, C. Empirical correlation between hydrophobic free energy and aqueous cavity surface area. *Proc. Natl Acad. Sci. USA* **71**, 2925–2927 (1974).
27. Richards, F. M. Areas, volumes, packing, and protein structure. *Annu. Rev. Biophys. Bioeng.* **6**, 151–176 (1977).
28. Sharp, K. A., Nicholls, A., Fine, R. F. & Honig, B. Reconciling the magnitude of the microscopic and macroscopic hydrophobic effects. *Science* **252**, 106–109 (1991).
29. Sharp, K. A., Nicholls, A., Friedman, R. & Honig, B. Extracting hydrophobic free energies from experimental data: relationship to protein folding and theoretical models. *Biochemistry* **30**, 9686–9697 (1991).
30. Böhm, H.-J. The development of a simple empirical scoring function to estimate the binding constant for a protein—ligand complex of known three-dimensional structure. *J. Comput. Aided Mol. Des.* **8**, 243–256 (1994).
31. Houk, K. N., Leach, A. G., Kim, S. P. & Zhang, X. Binding affinities of host–guest, protein– ligand, and protein–transition-state complexes. *Angew. Chem. Int. Ed.* **42**, 4872–4897 (2003).
32. Matsumoto, S., Iwamoto, H. & Mizutani, T. Water accessibility to the binding cleft as a major switching factor from entropy-driven to enthalpy-driven binding of an alkyl group by synthetic receptors. *Chem. Asian J.* **5**, 1163–1170 (2010).

33. Kojima, T. & Hiraoka, S. Selective alternate derivatization of the hexaphenylbenzene framework through a thermodynamically controlled halogen dance. *Org. Lett.* **16**, 1024–1027 (2014).
34. Kojima, T. & Hiraoka, S. Mesityllithium and p-(dimethylamino) phenyllithium for the selective alternate trilithiation of the hexaphenylbenzeneframework. *Chem. Commun.* **50**, 10420–10423 (2014).
35. Liao, J., Kojima, T., Takahashi, S. & Hiraoka, S. Gram-scale synthesis of a C_{2v} -symmetric hexaphenylbenzene with three different types of substituents. *Asian J. Org. Chem.* **7**, 2057–2060 (2018).
36. Lida, D. R. et al. CRC Handbook of Chemistry and Physics, 85th edn. (CRC Press, Boca Raton, 2005).
37. Dunitz, J. D. Win some, lose some: enthalpy–entropy compensation in weak intermolecular interactions. *Chem. Biol.* **2**, 709–712 (1995).
38. Sharp, K. Entropy–enthalpy compensation: fact or artifact? *Protein Sci.* **10**, 661–667 (2001).
39. Zhao, Y.-L., Houk, K. N., Rechavi, D., Scarso, A. & Rebek, J. Jr. Equilibrium isotope effects as a probe of nonbonding attractions. *J. Am. Chem. Soc.* **126**, 11428–11429 (2004).
40. Haino, T., Fukuta, K., Iwamoto, H. & Iwata, S. Noncovalent isotope effect for guest encapsulation in self-assembled molecular capsules. *Chem. Eur. J.* **15**, 13286–13290 (2009).
41. Turowski, M. et al. Deuterium isotope effects on hydrophobic interactions: the importance of dispersion interactions in the hydrophobic phase. *J. Am. Chem. Soc.* **125**, 13836–13849 (2003).
42. Kanao, E. Isotope effects on hydrogen bonding and CH/CD–Π interaction. *J. Phys. Chem. C.* **122**, 15026–15032 (2018).
43. Liu, Y. & Warmuth, R. Isotope effects as probe of constrictive and intrinsic binding in hemicarceplexes. *Org. Lett.* **9**, 2883–2886 (2007).
44. Wade, D. Deuterium isotope effects on noncovalent interactions between molecules. *Chem. Biol. Interact.* **117**, 191–217 (1999).
45. Liu, Y. & Warmuth, R. A "through–shell" binding isotope effect. *Angew. Chem. Int. Ed.* **44**, 7107–7110 (2005).
46. Felder, T. & Schalley, C. A. Secondary isotope effects on the deslipping reaction of rotaxanes: high–precision measurement of steric size. *Angew. Chem. Int. Ed.* **42**, 2258–2260 (2003).
47. Laughrey, Z. R., Upton, T. G. & Gibb, B. C. A deuterated deep-cavity cavitand confirms the importance of C–H···X–R hydrogen bonds in guest binding. Chem. Commun. 970–972 (2006).
48. Shi, C., Zhang, X., Yu, C.-H., Yao, Y.-F. & Zhang, W. Geometric isotope effect of deuteration in a hydrogen-bonded host–guest crystal. *Nat. Commun.* **9**, 481 (2018).
49. Bates, F. S., Keith, H. D. & McWhan, D. B. Isotope effect on the melting temperature of nonpolar polymers. *Macromolecules* **20**, 3065–3070 (1987).
50. Lacks, D. J. Origins of molar volume isotope effects in hydrocarbon systems. *J. Chem. Phys.* **103**, 5085–5090 (1995).
51. Allan, N. L., Barron, T. H. K. & Bruno, J. A. O. The zero static internal stress approximation in lattice dynamics, and the calculation of isotope effects on molar volumes. *J. Chem. Phys.* **105**, 8300–8303 (1996).
52. Rechavi, D., Scarso, A. & Rebek, J. Jr. Isotopomer encapsulation in a cylindrical molecular capsule: a probe for understanding noncovalent isotope effects on a molecular level. *J. Am. Chem. Soc.* **126**, 7738–7739 (2004).
53. Mugridge, J. S., Bergman, R. G. & Raymond, K. N. High-precision measurement of isotope effects on noncovalent host-guest Interactions. *J. Am. Chem. Soc.* **132**, 1182–1183 (2010).
54. Zhao, C. et al. Do deuteriums form stronger CH-Π interactions? *J. Am. Chem. Soc.* **134**, 14306–14309 (2012).
55. Matsuno, T., Fujita, M., Fukunaga, K., Sato, S. & Isobe, H. Concyclic CH-Π arrays for single-axis rotations of a bowl in a tube. *Nat. Commun.* **9**, 3779 (2018).
56. Kantonen, S. A., Henriksen, N. M. & Gilson, M. K. Evaluation and minimization of uncertainty in ITC binding measurements: heat error, concentration error, saturation, and stoichiometry. *Biochim. Biophys. Acta* **1861**, 485–498 (2017).
57. Shen, Z.-L., Xu, X.-P. & Ji, S.-J. Brønsted base-catalyzed one-pot three-component Biginelli-type reaction: an efficient synthesis of 4,5,6-triaryl-3,4-dihydropyrimidin-2(1H)-one and mechanistic study. *J. Org. Chem.* **75**, 1162–1167 (2010).
58. Hiraoka, S., Harano, K., Nakamura, T., Shiro, M. & Shionoya, M. Induced-fit formation of a tetrameric organic capsule consisting of hexagram-shaped amphiphile. *Angew. Chem. Int. Ed.* **48**, 7006–7009 (2009).
59. Case, D. A. et al. AMBER 14. http://ambermd.org/ (2014).
60. Wang, J. M., Wolf, R. M., Caldwell, J. W., Kollman, P. A. & Case, D. A. Development and testing of a general amber force field. *J. Comput. Chem.* **25**, 1157–1174 (2004).
61. Bayly, C. I., Cieplak, P., Cornell, W. & Kollman, P. A. A well-behaved electrostatic potential based method using charge restraints for deriving atomic charges: the RESP model. *J. Phys. Chem.* **97**, 10269–10280 (1993).
62. Frisch, M. J. et al. Gaussian 09, Revision A.02. http://gaussian.com/g09_a02/ (2009).
63. Joung, I. S. & Cheatham, T. E. Molecular dynamic simulations of the dynamic and energetic properties of alkali and halide ions using water-model-specific ion parameters. *J. Phys. Chem. B* **113**, 13279–13290 (2009).

Acknowledgements

This research was supported by JSPS Grants-in-Aid for Scientific Research on Innovative Areas "Dynamical Ordering of Biomolecular Systems for Creation of Integrated Functions" (25102001, 25102005, and 16H00780), the Mitsubishi Foundation, Sekisui Integrated Research and the Joint Research by Exploratory Research Center on Life and Living Systems (ExCELLS).

Author contributions

Y.-Y.Z., Q.-C.J., T.Koj., S.T., and S.H. conceived the project. S.H. prepared the manuscript and all the authors discussed the results and commented on the manuscript. Y.-Y.Z. and Q.-C.J. synthesized gear-shaped amphiphlies and measured NMR spectra and carried out ITC measurements. T.Koi., O.K., and M.T. carried out theoretical calculations. K.I. and S.U. carried out mass spectrometry of the nanocubes. Y.-Y.Z. carried out SAVPR for the nanocubes.

Competing interests

:The authors declare no competing interests.

Additional information

Supplementary information is available for this paper at https://doi.org/10.1038/s42004-019-0242-0.

Correspondence and requests for materials should be addressed to S.H.

Reprints and permission information is available at http://www.nature.com/reprints

Publisher's note Springer Nature remains neutral with regard to jurisdictional claims in published maps and institutional affiliations.